Peer reviewed Journals
seron press

RESEARCH

Bayesian Filtering of Two Phase Annular Flow with Solubility Mediated Mass Transfer and Vision Based Regime Identification

Juan Camilo[1] and Andres Felipe[2]

[1]Universidad del Magdalena, Carrera 32 No. 22-08, Santa Marta, Colombia
[2]Universidad de Nariño, Calle 18 No. 50-02 Ciudad Universitaria Torobajo, Pasto, Colombia

Abstract

Gas influx into a drilling annulus can evolve rapidly as it migrates upward through changing pressure, temperature, and hydrodynamic conditions. The resulting two-phase flow regimes are not only a consequence of the influx rate and gas properties but also of transient frictional losses, pipe eccentricity, and phase change driven by solubility. Reliable monitoring therefore requires models that remain predictive across regime transitions while remaining consistent with limited measurements available in operational settings. This paper develops a regime-aware digital twin that couples a reduced one-dimensional two-fluid formulation, a solubility-mediated mass-transfer model, and a probabilistic computer-vision regime identifier, enabling joint estimation of kick size, gas distribution, and evolving flow pattern from pressure and imaging data. The technical contribution is a unified latent-regime closure that is differentiable, smoothly switches interfacial momentum and friction correlations, and is constrained by conservation laws while remaining compatible with learning-based observation models. The approach explicitly represents dissolution and exsolution through a saturation-tracking state variable and leverages temporal visual features to infer regime probabilities with calibrated uncertainty. The overall inference problem is cast as a constrained Bayesian filtering task, where the physics model provides a predictive prior and computer vision provides a high-bandwidth likelihood over regime and void-fraction proxies. The framework is designed to generalize across static and circulating conditions, to accommodate gas-specific solubility effects, and to support mitigation-oriented control by predicting near-term pressure evolution under candidate actuation trajectories.

1. Introduction

Gas kicks in wellbores are fundamentally transient multiphase events in which a compressible, buoyant phase enters a confined vertical annulus and migrates upward under gravity while interacting with a moving or quiescent liquid phase [1]. Even when the inflow boundary condition is relatively simple, the ensuing dynamics quickly become high dimensional. The gas phase expands as hydrostatic pressure decreases with elevation, the liquid phase accelerates or decelerates depending on circulation and choke conditions, and interfacial momentum exchange changes as the flow reorganizes into distinct regimes such as dispersed bubbly, elongated bubble, churn-like structures, or intermittent configurations. These regime changes matter because the effective slip between phases, the interfacial area available for dissolution, and the frictional pressure gradient are all regime dependent [2]. In practice, monitoring and decision-making are commonly driven by pressure measurements, pit-volume changes, and surface flow signals. Yet these measurements are indirect and often insufficient to uniquely infer the evolving downhole gas distribution, particularly during the critical early period when mitigation choices have the largest impact.

A central challenge is that classical one-dimensional drift-flux or two-fluid models require closure relations that are sensitive to regime and geometry, while regime itself is rarely observed directly in field conditions. In an annulus, the geometry introduces additional complexity relative to a pipe [3]. The hydraulic diameter is not constant under eccentricity, and the gas phase can preferentially rise along the wider side, modifying apparent slip and creating azimuthal asymmetry that is difficult to capture with purely one-dimensional state variables. When circulation is present, additional frictional losses and liquid momentum can shift the onset of turbulence and alter the morphological evolution of the gas structure. Moreover, for soluble gases, dissolution at elevated pressure downhole and exsolution near the surface can change the effective gas volume fraction in ways that are not proportional to simple compressibility alone. These processes make it difficult to deploy models that are both computationally fast enough for real-time use and faithful enough to support safety-critical decisions [4].

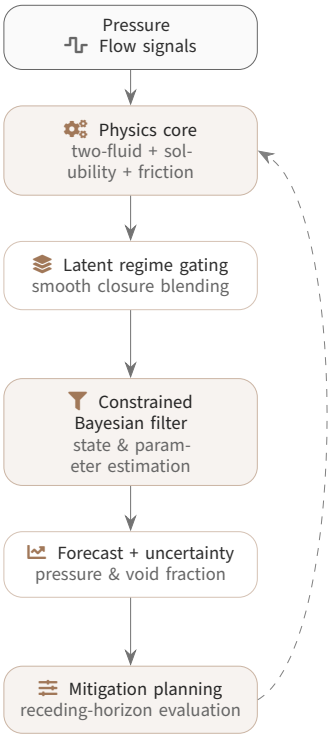


Figure 1. End-to-end regime-aware digital twin: pressure and video observations inform a latent regime field that gates slip, friction, and mass-transfer closures inside a reduced physics core, enabling Bayesian state estimation and mitigation-oriented forecasting.

This paper addresses the observability and closure problem by integrating physics-based modeling with computer-vision-based flow regime identification. The guiding thesis is that regime is best treated neither as an externally prescribed label nor as an unmodeled nuisance, but as a latent dynamical variable that can be inferred from visual evidence and used to condition physics closures in a differentiable, uncertainty-aware manner. The resulting digital twin treats regime as a probabilistic field over axial position and time, couples it to interfacial momentum exchange and wall friction, and constrains the overall evolution by conservation laws and thermodynamic solubility relations. The computational goal is not to replace mechanistic models with a purely data-driven surrogate, but to reduce the reliance on brittle heuristic regime maps by learning an observation model that informs regime probability directly from images while the physics model regularizes the inference through mass and momentum balance [5].

Laboratory experiments have demonstrated that regime evolution following an initial elongated-bubble signature can depend strongly on kick characteristics and geometry, including eccentricity effects and solubility-driven changes in gas availability; for example, controlled shut-in observations reported regime progression and turbulence onset variations under different injection histories and gas types in a tall annular setup [6]. Under circulating conditions, the interplay between frictional losses and liquid momentum further complicates the post-impact morphology, motivating closures that respond to evolving mixture velocity and not merely to initial kick parameters [7]. These empirical findings are consistent with the broader modeling view that regime-conditioned closures and solubility coupling are necessary for predictive migration forecasts. At the same time, recent availability of curated visual datasets of vertical annular two-phase regimes provides a pathway to learn robust image-to-regime mappings that can be integrated into real-time inference pipelines without abandoning physical constraints.

The contributions of this paper are organized around a unified formulation. A reduced two-fluid annular model is developed with explicit compressibility, dissolution, and frictional loss terms, designed to be discretized coarsely for fast prediction while preserving the dominant physics controlling pressure and void fraction [8]. A latent-regime gating mechanism is introduced to blend closure relations smoothly, avoiding discontinuities that destabilize filtering and gradient-based optimization. A temporal computer-vision model is proposed to infer regime probabilities and auxiliary continuous proxies from video streams, with uncertainty calibration to prevent overconfident regime switching when images are ambiguous or out of distribution. These components are fused through a constrained Bayesian filtering framework that estimates influx rate history,

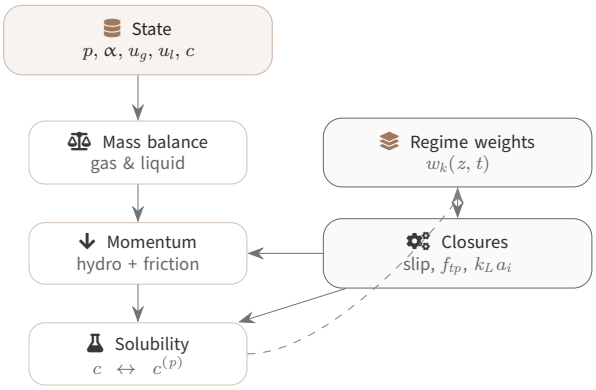


Figure 2. Reduced annular two-fluid model with an explicit dissolved-gas state. Latent regime weights gate slip, friction, and mass-transfer terms so that pressure and void-fraction dynamics remain consistent through transitions and solubility-driven phase exchange.

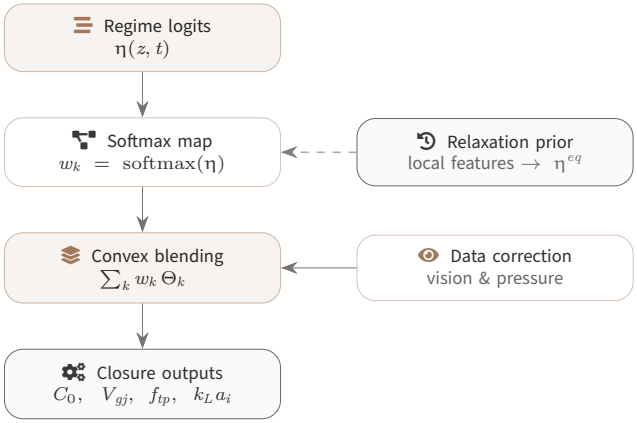


Figure 3. Differentiable latent-regime gating. Regime logits are mapped to simplex weights, then used to blend correlation parameters smoothly so slip, friction, and mass transfer can adapt continuously without hard switching.

gas distribution, and regime field while producing predictive intervals for pressure and void fraction. Finally, the digital twin is connected to mitigation-oriented control by embedding the predictor within a receding-horizon optimization that respects pressure safety constraints while accounting for regime-dependent friction and slip [9].

The remainder of the paper develops the approach in a self-contained manner. The physical phenomenology of annular gas migration is framed in terms of timescales, dimensionless groups, and geometry, emphasizing what must be captured by any reduced model. The governing equations are then presented with an emphasis on differentiable closure blending and solubility state tracking. The vision model is described as an observation module that outputs a calibrated distribution over regime and continuous flow descriptors rather than a single hard label [10]. Sensor fusion and state estimation are formulated as a constrained inference problem that can be implemented with particle filtering or ensemble smoothing. The final section ties the digital twin to mitigation-oriented control, showing how probabilistic regime inference and solubility coupling can alter predicted pressure trajectories and therefore decision margins.

2. Physical Setting and Phenomenology of Migrating Kicks

An annular gas kick begins with an influx event at some depth that introduces a compressible phase into a column of drilling fluid. The annulus is bounded internally by the drill pipe and externally by the casing or open hole, with a cross-sectional area that depends on diameters and any eccentricity [11]. Even in a nominally vertical configuration, eccentricity can be induced by contact and stiffness variations, causing the local gap width to vary azimuthally. This geometric nonuniformity influences both the liquid velocity profile and the gas rise pathway. Gas tends to migrate through the region of larger hydraulic radius, which can increase effective slip relative to concentric assumptions and can create intermittent coalescence and breakup as the gas phase interacts with shear gradients. While a fully resolved three-dimensional description would be ideal, operational constraints mo-

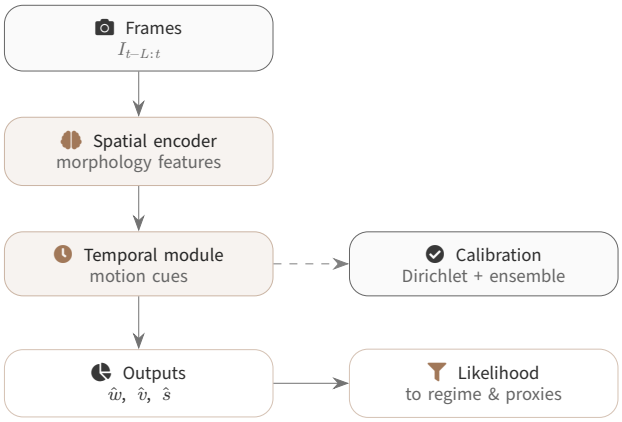


Figure 4. Computer-vision observation module. Spatiotemporal features yield a regime distribution and auxiliary continuous proxies, while calibration mechanisms provide uncertainty-aware likelihoods for fusion with the physics model.

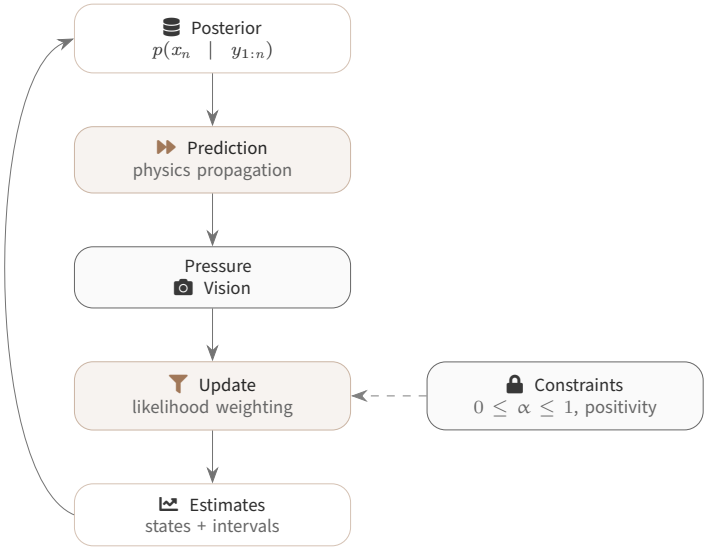


Figure 5. Sequential inference loop. The physics model supplies predictive priors, pressure and vision provide likelihood updates, and constraint-aware parameterizations preserve physical feasibility while producing uncertainty-calibrated estimates.

tivate reduced descriptions that must still encode the impact of geometry on friction and slip [12].

The morphological evolution of the gas phase is influenced by the initial influx characteristics but is not fully determined by them. The gas may initially appear as an elongated structure, particularly when injected through a restricted opening that encourages coalescence near the source. As the gas rises, pressure decreases, the gas expands, and the local void fraction can increase even if the mass of gas is unchanged. Expansion modifies both buoyancy and interfacial area, and the local mixture velocity can change due to continuity constraints and pressure-driven acceleration [13]. These effects can trigger transitions from dispersed bubbles to larger structures and to churn-like motion, especially when inertial forces dominate surface tension and when the void fraction crosses thresholds that destabilize uniform distributions. In an annulus, wall effects and the presence of two boundaries can stabilize or destabilize certain structures relative to a pipe, and the onset of slug-like intermittency can depend sensitively on eccentricity and on whether liquid circulation is present.

Solubility adds a second pathway by which the apparent gas volume fraction can change with elevation. A soluble gas can dissolve into the liquid phase at higher pressure, reducing free-gas volume, and then exsolve as pressure decreases near the surface [14]. This produces a hysteretic behavior in which the free-gas fraction depends on both the current pressure and the prior exposure history of the liquid to gas. When the liquid is not saturated, dissolution can significantly delay the growth of void fraction as the gas rises. When the liquid becomes saturated at depth, subsequent pressure drop can release gas rapidly, increasing bubble nucleation and potentially shifting the regime toward

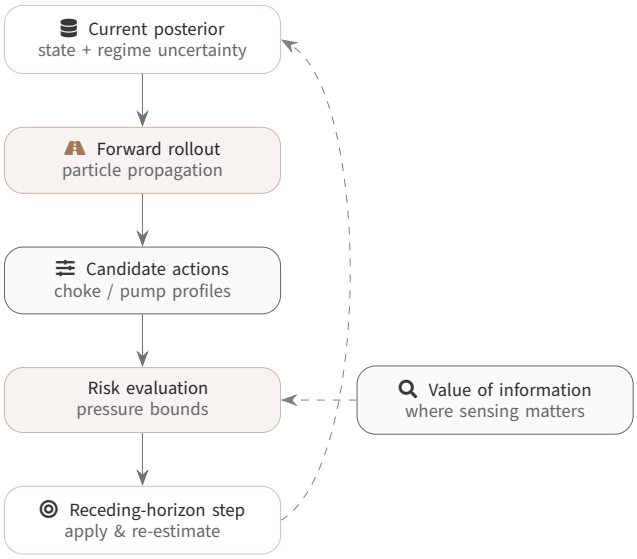


Figure 6. Mitigation-oriented use of the digital twin. Posterior particles are rolled forward under candidate actuation trajectories to evaluate constraint risk under regime-dependent slip, friction, and solubility effects, supporting receding-horizon decision-making.

more dispersed and agitated structures near the top of the column [15]. The timescale of mass transfer depends on interfacial area, turbulence, and molecular diffusivity, all of which are regime dependent. A reduced model therefore requires at least a minimal state representation of dissolved gas content and a coupling between regime and effective mass-transfer coefficients.

Dynamic conditions during drilling or circulation introduce additional momentum exchange and frictional losses. Liquid circulation imposes a baseline mixture velocity that can suppress buoyancy-driven segregation in some regimes and enhance turbulence and breakup in others [16]. Frictional pressure gradient is not simply proportional to mixture velocity because it is influenced by effective viscosity, phase distribution near walls, and intermittent acceleration events in churn-like motion. In a circulating annulus, the same amount of gas mass can lead to different surface pressure signatures depending on how quickly the gas is transported, how strongly it slips, and how it redistributes across the cross section. These dependencies complicate the inverse problem of estimating kick size from limited surface measurements, since multiple internal configurations can be consistent with similar pressure traces.

From a modeling perspective, the key phenomenological requirement is to represent the coupled evolution of pressure, void fraction, and slip in a way that is robust to regime transitions and to partial dissolution [17]. A second requirement is to represent the effect of annular geometry and eccentricity on friction and slip without requiring azimuthal resolution. A third requirement is observability: since regime and void fraction are not directly measured downhole in many scenarios, the model must be able to incorporate additional data streams when available, such as imaging in laboratory settings or potentially acoustic or resistivity proxies in field settings. In the present framework, visual information is treated as a high-bandwidth observation that can anchor regime inference, enabling the physical model to use regime-conditioned closures without relying exclusively on heuristics.

The phenomenology also motivates a probabilistic treatment [18]. Regime transitions are not deterministic thresholds; they can occur over ranges of conditions with stochastic variability due to turbulence and local perturbations. A hard regime map with abrupt switching can produce numerical instability and unrealistic oscillations in predicted pressure gradients, which in turn degrade filtering. A smooth, probabilistic regime field allows the digital twin to express uncertainty and to avoid overcommitting to a single closure when evidence is weak. This is particularly important during transitions, where small changes in void fraction or mixture velocity can alter the dominant interfacial structures [19]. By encoding regime as a latent variable inferred from data, the model can adapt its closures continuously while quantifying the confidence of that adaptation.

3. Regime-Aware Reduced Two-Fluid Model with Solubility Coupling

The digital twin is built around a one-dimensional annular two-fluid formulation that resolves axial variations while representing cross-sectional complexity through effective parameters. Let z denote measured depth (positive upward for convenience) and t denote time. The annular cross-sectional area is A, and the wetted perimeter is P, yielding a hydraulic diameter $D_h =$

Table 1. Core components of the regime-aware digital twin

Module	Purpose	Main ingredients
Reduced two-fluid core	1D annular mass and momentum balance	Compressible gas, weakly compressible liquid, drift-flux slip, two-phase friction
Solubility coupling	Track dissolution and exsolution of gas	Dissolved mass fraction c, equilibrium curve $c^*(p)$, regime-dependent mass-transfer rate $\dot{m}_{tr}$
Latent-regime field	Smoothly condition closures on morphology	Regime logits η, softmax weights w_k, relaxation toward equilibrium map $\eta^{eq}(q)$
Vision observation model	Infer regime and flow descriptors from video	Spatiotemporal features, regime probabilities $\hat{w}$, void-fraction proxy $\hat{v}$, intermittency score $\hat{s}$
Bayesian state estimator	Fuse physics model with heterogeneous sensing	Particle / ensemble filtering, constrained state transforms, likelihoods for pressure and vision
Prediction and control	Evaluate mitigation actions under uncertainty	Scenario propagation of particles, risk-sensitive cost functional, comparison of candidate actuation trajectories

$4A/P$ [20]. Eccentricity and pipe movement can be represented through a time-varying effective $D_h(t)$ and through a correction factor in the friction closure, allowing the model to capture first-order geometric impacts without azimuthal resolution.

Define $\alpha(z,t)$ as the gas void fraction, $u_g(z,t)$ and $u_l(z,t)$ as phasic average velocities, $\rho_g(p)$ as the gas density, and ρ_l as the liquid density, treated as weakly compressible over the pressure range of interest. The dissolved gas mass fraction in the liquid is represented by $c(z,t)$, defined as mass of dissolved gas per mass of liquid. The free-gas pressure is taken equal to mixture pressure $p(z,t)$ under the assumption of negligible capillary pressure at the reduced-model scale, with surface tension effects absorbed into regime-dependent slip and mass-transfer closures [21].

Mass conservation for each phase is expressed as

$$\frac{\partial}{\partial t}(\alpha\rho_g) + \frac{\partial}{\partial z}(\alpha\rho_g u_g) = s_g(z,t) - \dot{m}_{tr}(z,t), \tag{1}$$

$$\frac{\partial}{\partial t}((1-\alpha)\rho_l) + \frac{\partial}{\partial z}((1-\alpha)\rho_l u_l) = s_l(z,t) + \dot{m}_{tr}(z,t), \tag{2}$$

where s_g and s_l represent any distributed sources or sinks such as influx at depth or leak-off, and $\dot{m}_{tr}$ is the interphase mass-transfer rate per unit volume that accounts for dissolution and exsolution. In many kick scenarios, s_g is concentrated near the influx depth and is zero elsewhere, while s_l is determined by circulation boundary conditions. The dissolved-gas state satisfies a transport equation consistent with liquid advection and interphase transfer:

$$\frac{\partial}{\partial t}((1-\alpha)\rho_l c) + \frac{\partial}{\partial z}((1-\alpha)\rho_l c\, u_l) = \dot{m}_{tr}(z,t) - \dot{m}_{loss}(z,t), \tag{3}$$

where $\dot{m}_{loss}$ can represent irreversible processes such as gas leaving the liquid through microbubble escape at the surface, though it is typically negligible in a closed annulus segment and can be used primarily to regularize boundary layers in simulation.

The momentum balance is expressed in mixture form with a regime-conditioned slip relation [?]. Define mixture density $\rho_m = \alpha\rho_g + (1-\alpha)\rho_l$ and mixture velocity $u_m = \alpha u_g + (1-\alpha)u_l$. A reduced momentum equation that captures hydrostatic, frictional, and acceleration terms is

$$\frac{\partial}{\partial t}(\rho_m u_m) + \frac{\partial}{\partial z}\left(\rho_m u_m^2\right) + \frac{\partial p}{\partial z} + \rho_m g \tag{4}$$

$$= -\frac{f_{tp}}{2D_h}\,\rho_m u_m |u_m| + \phi_{slip}(z,t). \tag{5}$$

where g is gravitational acceleration, f_{tp} is an effective two-phase friction factor, and ϕ_{slip} captures residual momentum exchange effects not represented in mixture form, including drift contributions that arise when phasic velocities differ significantly. In implementa-

Table 2. Selected notation for the reduced annular model

Symbol	Description	Units / type
z	Measured depth (positive upward)	m
t	Time	s
A, P	Annular cross-sectional area and wetted perimeter	m^2, m
D_h	Hydraulic diameter $4A/P$ (eccentricity-effective)	m
α	Gas void fraction	–
u_g, u_l, u_m	Gas, liquid, and mixture velocities	m/s
p, c, ρ_m	Mixture pressure, dissolved-gas mass fraction, mixture density	Pa, –, kg/m^3

Table 3. Key physical phenomena influencing annular gas-kick migration

Phenomenon	Effect on migration	Representation in model
Gas compressibility	Expansion as pressure decreases, changing buoyancy and void fraction	Pressure-dependent density $\rho_g(p)$ in mass balance and momentum equations
Buoyancy and slip	Relative rise of gas against liquid, modifying transport speed	Drift-flux relation $j_g = C_0(r)\,\alpha j_m + V_{gj}(r)\,\alpha$
Annular geometry and eccentricity	Asymmetric pathways and modified friction	Effective $D_h(t)$ and eccentricity factor in two-phase friction closure f_{tp}
Solubility of gas in liquid	Dissolution at depth and exsolution near surface	State variable c, equilibrium $c^*(p)$, transfer term $\dot{m}_{tr} \propto k_L(r)a_i(\alpha, r)(c^* - c)$
Circulation and frictional losses	Additional momentum input and pressure drop	Boundary conditions on u_l, regime-aware friction factor $f_{tp}(\alpha, r, Re_m)$
Intermittent / churn-like motion	Enhanced fluctuations and energy dissipation	Regime-dependent friction blending and pressure-variance proxy $\sigma_p^2(z, t)$

tions aimed at real-time inference, ϕ_{slip} is often absorbed into the slip closure by defining a drift-flux relation and computing u_g and u_l accordingly, thereby keeping a single momentum equation and reducing stiffness.

Slip is introduced through a regime-aware drift relation. Let superficial velocities be $j_g = \alpha u_g$ and $j_l = (1-\alpha)u_l$, and define $j_m = j_g + j_l = u_m$ in the present normalization [22]. The drift-flux form is written as

$$j_g = C_0(r)\,\alpha\, j_m + V_{gj}(r)\,\alpha, \tag{6}$$

where $C_0(r)$ and $V_{gj}(r)$ depend on a latent regime variable $r(z,t)$ that encodes morphological state. This form allows the model to represent increased slip in elongated-bubble or churn-like structures through larger V_{gj}, while dispersed bubbly regimes can be represented with smaller drift velocity and different distribution parameter C_0. The dependence on r will be made explicit through a smooth gating mechanism that blends parameter sets associated with canonical regimes.

Solubility coupling enters through $\dot{m}_{tr}$, which is modeled as a relaxation toward equilibrium governed by Henry-type solubility and a regime-dependent interfacial area. Let $c^*(p)$ denote the equilibrium dissolved-gas mass fraction at pressure p for the gas–liquid pair under consideration. The equilibrium is approached via [23]

$$\dot{m}_{tr} = k_L(r)\; a_i(\alpha, r)\; \rho_l \left(c^*(p) - c\right), \tag{7}$$

with $k_L(r)$ an effective liquid-side mass-transfer coefficient and $a_i(\alpha, r)$ an interfacial area density. This form allows dissolution when $c < c^*(p)$ and exsolution

Table 4. Canonical flow regimes and qualitative closure behavior

Regime	Morphology	Slip / friction traits	Interfacial area trend
Dispersed bubbly	Many small bubbles in continuous liquid	Modest slip, friction close to liquid-dominated	High area density, strong dissolution potential
Elongated bubble	Large bullet-like gas structures	Higher slip, reduced wall wetted by liquid	Lower area per gas volume than bubbly flow
Churn-like	Agitated, rapidly breaking / coalescing gas pockets	Strong fluctuations, enhanced effective friction	Intermediate area, strongly time-varying
Intermittent / slug	Alternating gas-rich and liquid-rich segments	Large pressure oscillations, regime-dependent slip	Area modulated by slug structure and film thickness

Table 5. Latent-regime gating and blended closures

Closure quantity	Blending expression	Primary effect on dynamics
Distribution parameter $C_0(r)$	$\sum_k w_k C_{0,k}$	Controls partition of mixture flux between gas and liquid
Drift velocity $V_{gj}(r)$	$\sum_k w_k V_{gj,k}$	Sets slip between phases and gas rise speed
Two-phase friction $f_{tp}(r)$	Blended via dissipation density $\mathcal{D} = \sum_k w_k \mathcal{D}_k$	Determines frictional pressure gradient and energy loss
Mass-transfer coefficient $k_L(r)$	$\sum_k w_k k_{L,k}$	Modulates rate of dissolution and exsolution
Interfacial area $a_i(\alpha, r)$	$\sum_k w_k a_{i,k}(\alpha)$	Couples morphology to available area for mass transfer
Pressure-variance proxy σ_p^2	Source term $\propto \beta_\sigma(r)\rho_m^2 u_m^4$	Encodes regime-dependent intermittency in the likelihood model

when $c > c^*(p)$, thereby capturing hysteresis through the state variable c. In practice, exsolution can be limited by nucleation kinetics and may require supersaturation; such effects can be represented by replacing $(c^*(p) - c)$ with a smoothed function that delays exsolution until c exceeds $c^*(p)$ by a small threshold. The threshold is not treated as a fixed constant but as a regime-dependent parameter, since turbulence and existing bubbles facilitate exsolution by providing nucleation sites [24].

The reduced model must also close f_{tp}. A regime-aware friction factor is expressed as a blend between a liquid-dominated friction factor f_l and a gas-affected factor f_g, with additional dependence on void fraction:

$$f_{tp}(\alpha, r, Re_m) = \lambda(r)\, f_{mix}(\alpha, Re_m) + \big(1 - \lambda(r)\big)\, f_{int}(\alpha, Re_m), \tag{8}$$

where $Re_m = \rho_m |u_m| D_h / \mu_{eff}$ is an effective mixture Reynolds number based on an effective viscosity μ_{eff}, and f_{mix} and f_{int} represent alternative parameterizations suitable for dispersed versus intermittent morphologies. The blending coefficient $\lambda(r)$ is derived from the same latent regime field used for slip, ensuring consistent closure switching. Eccentricity effects can be embedded by allowing D_h and a correction factor κ_e to modify the friction term as $f_{tp}/D_h \mapsto \kappa_e f_{tp}/D_h$, where κ_e can be inferred or bounded based on known geometry.

To make the model computationally tractable for inference, spatial discretization is performed on a coarse grid in z with conservative fluxes, and the latent regime field is represented per cell [25]. The governing equations are integrated using a semi-implicit scheme for the pressure and mass-transfer terms to handle stiffness introduced by gas compressibility and rapid dissolution near equilibrium. Differentiability is maintained by using smooth approximations for absolute values and by avoiding hard regime switches, enabling gradient-based parameter adaptation and enabling the vision model outputs to influence closures continuously.

Table 6. Computer-vision observation outputs and their roles

Output	Type	Use in digital twin
Regime weights $\hat{w}$	Probability vector on simplex	Likelihood term for latent logits η, informs closure blending
Void-fraction proxy $\hat{v}$	Continuous estimate from segmentation or texture	Anchors axial evolution of α through a noisy observation model
Intermittency score $\hat{s}$	Scalar derived from temporal variation	Guides regime preference toward churn-like or slug-like states
Aleatoric uncertainty	Frame-specific confidence indicator	Modulates concentration parameter κ_v in regime likelihood
Epistemic uncertainty	Ensemble- or dropout-based spread	Downweights vision influence under domain shift

Table 7. Main state components in the Bayesian filtering formulation

State component	Representation	Notes
Pressure $p(z)$	Discretized over axial grid	Constrained by mass and momentum balance, observed at sensor depths
Void fraction $\alpha(z)$	Logistic transform of unconstrained variable	Bounded between 0 and 1, strongly coupled to slip and friction
Dissolved-gas fraction $c(z)$	Saturating transform to enforce physical bounds	Encodes solubility memory and hysteresis along the column
Mixture / phasic velocities	$u_m(z)$ (and derived u_g, u_l)	Driven by boundary conditions, friction, and gas expansion
Regime logits $\eta(z)$	Low-dimensional latent field	Advected and relaxed, corrected by visual observations
Influx and geometry parameters	Basis coefficients for $q_g(t)$, factor κ_e	Capture kick history and effective eccentricity in a low-dimensional form

4. Latent-Regime Gating and Differentiable Closure Blending

A core difficulty in regime-aware multiphase modeling is that regime boundaries are not sharply defined, and hard switching between closure correlations can produce discontinuous flux Jacobians that destabilize both time integration and data assimilation. To address this, regime is represented by a continuous latent variable $r(z,t)$ mapped to a simplex of regime weights [26]. Consider a set of K canonical regimes, each associated with a parameter tuple Θ_k that defines C_0, V_{gj}, k_L, and friction parameters. The model defines regime weights $w_k(z,t)$ satisfying $\sum_{k=1}^{K} w_k = 1$ and $w_k \geq 0$, and constructs closures as convex combinations:

$$C_0(r) = \sum_{k=1}^{K} w_k \, C_{0,k}, \tag{9}$$

$$V_{gj}(r) = \sum_{k=1}^{K} w_k \, V_{gj,k}, \tag{10}$$

$$k_L(r) = \sum_{k=1}^{K} w_k \, k_{L,k}, \tag{11}$$

$$f_{tp}(r) = \sum_{k=1}^{K} w_k \, f_{tp,k}. \tag{12}$$

The weights are generated from a low-dimensional regime logit vector $\eta(z,t) \in \mathbb{R}^K$ using a softmax map, $w_k = \exp(\eta_k)/\sum_j \exp(\eta_j)$. The logits evolve according to a

Table 8. Prediction and mitigation-oriented quantities of interest

Quantity	Description	Dependence on regime and solubility
Control trajectory $u(t)$	Pump rate, choke settings, circulation strategy	Alters mixture velocity, frictional losses, and pressure levels
Bottomhole pressure $p_{bh}(t)$	Pressure near influx depth	Sensitive to gas expansion, dissolution at depth, and friction profile
Casing-shoe pressure $p_{shoe}(t)$	Representative structural load	Affected by regime-dependent pressure gradient above the shoe
Near-surface void fraction $\alpha_{surf}(t)$	Gas presence in upper annulus segment	Influenced by slip, exsolution, and morphology near the surface
Risk-sensitive cost $J(u)$	Expected penalty over horizon	Aggregates probability of pressure violations and high gas fraction under uncertainty

relaxation dynamics that encourages consistency with local hydrodynamic conditions while allowing data-driven correction:

$$\frac{\partial \eta}{\partial t} + u_m \frac{\partial \eta}{\partial z} = -\frac{1}{\tau_r}\left(\eta - \eta^{eq}(q)\right) + \xi(z,t), \tag{13}$$

where τ_r is a regime adaptation timescale, $q(z,t)$ is a vector of local features derived from the physical state, $\eta^{eq}(q)$ is a smooth equilibrium mapping, and ξ is a correction term supplied by data assimilation. The feature vector q may include void fraction, mixture Reynolds number, Froude-like groups based on $u_m^2/(gD_h)$, and a capillary-related group based on effective surface tension. Importantly, $\eta^{eq}(q)$ is not a hard regime map. It is a smooth function implemented as a small differentiable network or as an analytic regression that outputs logits rather than labels, ensuring continuity.

This latent-regime equation serves two roles [27]. It provides a physically plausible prior evolution for regime, preventing the vision module from causing rapid, spatially incoherent switching due to noise. It also allows the assimilation algorithm to treat regime as a state variable rather than a static classification, enabling temporal smoothing and uncertainty quantification. The regime timescale τ_r can be interpreted as the time required for morphological reorganization under local shear and buoyancy conditions; it is expected to decrease under high turbulence and increase under quiescent conditions. This dependence can be encoded by setting $\tau_r = \tau_0/(1+\chi Re_m^{\gamma})$ with parameters τ_0, χ, γ inferred from data [28].

The interfacial area term $a_i(\alpha, r)$ is a primary channel through which regime affects dissolution and exsolution. A dispersed bubbly regime typically has high interfacial area per unit volume, while elongated bubbles reduce area density for the same void fraction. A differentiable parameterization is

$$a_i(\alpha, r) = \sum_{k=1}^{K} w_k\, a_{i,k}(\alpha), \quad a_{i,k}(\alpha) = \frac{6\alpha}{d_{b,k}(\alpha)}\,\sigma_k(\alpha), \tag{14}$$

where $d_{b,k}(\alpha)$ is an effective bubble diameter function in regime k and $\sigma_k(\alpha)$ is a smooth saturation factor that prevents unphysical growth as $\alpha \to 1$. In elongated-bubble regimes, $d_{b,k}$ is replaced by an equivalent hydraulic length scale tied to D_h, yielding reduced a_i and hence slower dissolution for a given α. This coupling captures a key mechanism by which morphology influences solubility-mediated dynamics, namely that the same gas mass can produce different dissolved-gas uptake depending on whether it is dispersed into many small bubbles or concentrated into large structures [29].

The friction closure blending is designed to preserve monotonicity of pressure drop with respect to mixture velocity in the range of interest. If $f_{tp,k}$ are parameterized in a way that can violate monotonicity when blended, the model can produce spurious accelerations during transitions. To mitigate this, friction is blended at the level of an energy dissipation term rather than directly blending friction factors. Define a dissipation density $\mathcal{D}_k = (f_{tp,k}/2D_h)\,\rho_m u_m|u_m|$, and blend $\mathcal{D} = \sum_k w_k \mathcal{D}_k$, then recover an effective friction factor $f_{tp} = 2D_h\mathcal{D}/(\rho_m u_m|u_m| + \epsilon)$ with a small ϵ for differentiability near $u_m = 0$. This approach makes the friction term convex in the regime weights and reduces the risk of nonphysical negative dissipation.

A related issue is the representation of intermittent

Table 9. Selected modeling and inference challenges with mitigation strategies

Challenge	Source	Mitigation strategy
Ill-posed inverse from pressure only	Multiple gas distributions fit similar pressure traces	Introduce latent regime field and dissolved state, use Bayesian filtering with uncertainty
Regime transition ambiguity	Non-unique thresholds and stochastic variability	Use continuous logits η with softmax weights and relaxation dynamics instead of hard maps
Solubility parameter uncertainty	Limited data on $c^*(p)$ and k_L for specific fluids	Treat solubility parameters as uncertain, infer from data with conservative priors
Vision domain shift	Different fluids, geometries, or optics than training set	Calibrated uncertainty, ensemble predictions, and physics-based regularization of regime
Unresolved intermittency	Coherent oscillations not captured by coarse grid	Statistical treatment via variance proxy σ_p^2 and inflated model error
Numerical stiffness	Coupled compressibility, mass transfer, and closures	Semi-implicit time integration and smooth, differentiable closure formulations

pressure signatures associated with churn-like motion [30]. A fully resolved model would require capturing large-scale oscillations and local accelerations. In a reduced model, these effects are represented statistically through an additive pressure-gradient variance term that informs uncertainty in predictions rather than altering the mean dynamics directly. Let $\sigma_p^2(z,t)$ denote a local variance proxy driven by regime and mixture velocity:

$$\frac{\partial \sigma_p^2}{\partial t} + u_m \frac{\partial \sigma_p^2}{\partial z} = -\frac{1}{\tau_\sigma}\,\sigma_p^2 + \beta_\sigma(r)\,\rho_m^2 u_m^4, \tag{15}$$

where $\beta_\sigma(r)$ increases for intermittent regimes [31]. This variance proxy is used in the Bayesian filter likelihood to prevent overfitting pressure data when intermittent dynamics are present but unresolved at the model scale.

The latent-regime closure blending is thus not merely a numerical trick but a modeling stance: regime is treated as a continuous, uncertain field that shapes slip, friction, and mass transfer. The blending is differentiable, enabling end-to-end calibration and making it compatible with modern learning-based observation models. The next section describes how computer vision provides such observations and how it can be integrated without forcing the paper to hinge on any single dataset [32].

5. Computer Vision Observation Model for Flow-Regime Identification

Visual sensing provides a direct view of the morphology that regime-aware closures attempt to represent. Even when field deployment is constrained, laboratory datasets and controlled experiments provide a pathway to develop and validate image-based regime inference modules that can later be adapted to other sensing modalities. The vision component in the present framework is designed as an observation model that outputs a probability distribution over regimes and continuous auxiliary descriptors such as a void-fraction proxy and an intermittency index. These outputs are treated as noisy measurements that constrain the latent regime field and, indirectly, the slip and friction closures [33].

The observation model is trained and evaluated using a curated annular two-phase image dataset capturing regime transitions in a vertical tower configuration, with high-resolution imagery intended to support machine-vision development for regime detection [34]. The dataset's focus on vertical conditions and its omission of certain extreme regimes motivates design choices aimed at generalization rather than overspecialization. In particular, the vision model is constructed to rely on spatiotemporal texture and motion cues that are stable across moderate domain shifts, and it is equipped with uncertainty mechanisms to recognize when inputs are outside the training distribution.

Let $I_{t-L:t}$ denote a short temporal window of images. The vision model defines

$$\hat{w}(z,t),\ \hat{v}(z,t),\ \hat{s}(z,t) = \mathcal{V}_\theta(I_{t-L:t})\,, \tag{16}$$

where $\hat{w}$ is a predicted regime weight vector on the simplex, $\hat{v}$ is a continuous void-fraction proxy, and $\hat{s}$ is an intermittency score. The architecture is chosen to cap-

ture both spatial morphology and temporal evolution [35]. A practical choice is a convolutional backbone for spatial feature extraction followed by a temporal transformer or gated recurrent unit that aggregates motion information without assuming periodicity. The temporal component is important because still images can be ambiguous between certain regimes that differ primarily in dynamics, such as slowly varying slug-like structures versus churn with rapid breakup and coalescence. The model is trained with a combination of supervised regime labels and self-supervised temporal consistency losses that encourage stable predictions under small time shifts.

Because regime classification errors can have outsized effects when used to gate physical closures, calibration is essential [36]. The model therefore outputs not only point estimates but also uncertainty. Two complementary uncertainty types are represented. Aleatoric uncertainty captures inherent ambiguity due to occlusion, lighting, or morphological overlap; it is modeled by predicting a concentration parameter for a Dirichlet distribution over regime weights, enabling the model to express diffuse beliefs when evidence is weak [37]. Epistemic uncertainty captures model uncertainty under domain shift; it is approximated using an ensemble of networks or stochastic dropout at inference time, producing a distribution over outputs. The digital twin uses these uncertainty estimates to temper the influence of vision during assimilation, preventing abrupt closure changes when the vision model is uncertain.

To connect visual cues to physically meaningful proxies, the model includes auxiliary heads trained on continuous targets derived from image statistics when direct void-fraction ground truth is unavailable. For example, the fraction of pixels classified as gas-like under a learned segmentation can serve as a monotone proxy for void fraction under fixed lighting and geometry [38]. Even if not absolutely calibrated, such proxies provide valuable constraints on axial evolution when combined with pressure measurements. The model also predicts an intermittency score based on frame-to-frame variation in segmentation maps and optical flow magnitude, capturing the temporal variability that is characteristic of churn-like motion. These auxiliary outputs are not treated as definitive measurements but as informative cues that reduce ambiguity in the physical inverse problem.

A key concern is that the dataset used for training may not include soluble-gas effects, non-Newtonian drilling fluids, or eccentric annular geometries that appear in broader applications [39]. The framework addresses this by emphasizing domain-robust feature learning and by providing a pathway for physics-guided augmentation. Synthetic image generation from computational fluid simulations can be used to diversify morphological patterns, but even without photorealistic rendering, texture and motion statistics can be perturbed through controlled transformations that preserve regime semantics. The model is also trained with invariances to illumination, contrast, and mild geometric distortions to reduce sensitivity to camera placement. When the vision module is deployed in a new domain, its epistemic uncertainty acts as a safeguard, reducing its weight in assimilation until adaptation data are available [40].

Finally, the vision module is integrated into the digital twin as a likelihood function. If $\eta(z,t)$ are the latent regime logits, then the vision observation can be modeled as

$$p(\hat{w} \mid \eta) \propto \mathrm{Dirichlet}(\hat{w};\, \kappa_v \,\mathrm{softmax}(\eta))\,, \tag{17}$$

$$p(\hat{v} \mid \alpha) = \mathcal{N}\Big(\hat{v};\, h_v(\alpha),\, \sigma_v^2\Big)\,. \tag{18}$$

with κ_v reflecting confidence and h_v mapping void fraction to the proxy space. The dependence of κ_v on predicted uncertainty ensures that ambiguous frames exert less influence [41]. This probabilistic interface allows the vision module to inform regime inference without dictating it, preserving a balance between data-driven evidence and physics-based constraints.

6. Bayesian Sensor Fusion and Real-Time State Estimation

The digital twin's operational value depends on its ability to estimate hidden states and uncertain parameters from limited measurements. The state includes pressure $p(z,t)$, void fraction $\alpha(z,t)$, dissolved-gas fraction $c(z,t)$, mixture velocity $u_m(z,t)$ or superficial velocities, and regime logits $\eta(z,t)$. Additional parameters may include effective eccentricity correction κ_e, inflow boundary conditions for gas and liquid, and gas-specific solubility parameters embedded in $c^*(p)$ [42]. The estimation goal is to infer the posterior distribution over these quantities given time-series measurements such as pressure at discrete sensor depths, surface flow rates, and vision outputs when available.

Let the discretized state vector at time step n be x_n, and let the measurement vector be y_n. The physics model provides a transition density

$$x_{n+1} = \mathcal{F}(x_n, u_n) + \omega_n, \tag{19}$$

where u_n denotes known inputs such as pump rate or choke setting, and ω_n represents model error, including unresolved intermittency and uncertain closures [43]. Measurements satisfy

$$y_n = \mathcal{H}(x_n) + \nu_n, \tag{20}$$

where $\mathcal{H}$ extracts pressure at sensor locations and includes the vision likelihood described earlier. The posterior $p(x_n \mid y_{1:n})$ is propagated sequentially.

A particle filtering approach is attractive because the dynamics are nonlinear and regime uncertainty can

produce multimodal posteriors. Each particle carries a full state realization including regime logits. The transition step advances the reduced model using the particle's parameters and states [44]. The update step weights particles by the likelihood of observed pressures and vision outputs. To avoid particle degeneracy when the state dimension is large, the filter leverages structure: regime logits are updated using a conditional move that combines the relaxation prior with a gradient-informed correction from the vision likelihood, while the physical variables are nudged through an ensemble Kalman-like affine update conditioned on pressure residuals. This hybrid approach preserves the ability to represent multimodality in regime while exploiting approximate Gaussian structure in pressure-driven corrections.

The assimilation must respect physical constraints such as $0 \le \alpha \le 1$, positivity of densities, and saturation bounds on dissolved gas [45]. Constraint handling is implemented through smooth transformations. Void fraction is represented via a logistic map $\alpha = \sigma(\zeta)$ with unconstrained ζ, and regime weights are represented via softmax logits. Dissolved fraction c is represented via a saturating transform that enforces nonnegativity and caps c at a maximum physically plausible value linked to $c^*(p)$ under maximum pressure. These transforms ensure that filter updates cannot produce unphysical states that would destabilize the forward model [46].

Kick characterization is naturally expressed in terms of an unknown influx history at depth. Rather than estimating a single scalar kick volume, the framework estimates a low-dimensional parameterization of the inflow rate $q_g(t)$ over a recent time window. This parameterization can be expressed as a smooth basis expansion whose coefficients are included in the state. The filter then infers these coefficients by matching pressure and regime observations [47]. This approach accommodates the fact that influx can be intermittent and that surface signatures depend on both total mass and timing. The inferred inflow history also supports predictive forecasting because it provides a consistent initial condition for forward simulation.

A major benefit of including solubility and the dissolved-gas state is improved identifiability of gas mass under conditions where free-gas volume is suppressed at depth [48]. In purely compressible models without dissolution, early-time pressure responses can be misattributed to small influxes because the free gas is assumed to remain free and therefore expands more rapidly. By tracking c and allowing dissolution, the model can represent scenarios where a significant amount of gas mass is temporarily hidden in solution, delaying void-fraction growth. The filter can then use later exsolution signatures, such as increased visual bubble density or changes in pressure gradient near the surface, to revise estimates of the earlier influx. This temporal coupling produces more consistent posteriors, particularly when the available sensors are sparse [49].

The probabilistic regime field also acts as an explanatory variable for pressure residuals. If the model predicts a pressure gradient that is too low, a plausible explanation is that the true regime is more intermittent or churn-like than assumed, which would increase friction and alter slip. Rather than forcing a correction solely through void fraction or inflow rate, the filter can adjust regime logits to explain pressure differences while keeping mass conservation intact. This reduces the risk of compensating errors in which the model overestimates gas volume to match pressure drop when the true discrepancy arises from friction closure mismatch [50].

Real-time viability is achieved by keeping the state dimension modest through coarse axial discretization and by using efficient forward integration. The regime logits can be represented at the same grid resolution as pressure, and the vision likelihood can be computed at the camera's axial location, optionally augmented by a short axial footprint if the camera observes a segment. The overall computation scales linearly with the number of grid cells and particles. For scenarios in which only pressure data are available, the vision module is simply omitted and the regime evolves according to the relaxation prior, with increased uncertainty reflected in broader posterior distributions over regime and closures [51].

7. Mitigation-Oriented Prediction and Control Under Regime Uncertainty

A digital twin that estimates current state is most valuable when it can predict near-term evolution under candidate mitigation actions. In drilling contexts, actions may include adjusting choke pressure, changing pump rate, or modifying circulation strategy. The aim is to keep bottomhole and casing pressures within safe margins while transporting the influx in a controlled manner. This paper treats control at a conceptual algorithmic level, focusing on how regime-aware modeling and solubility coupling affect predictions and thereby influence decision margins, rather than prescribing operational procedures [52].

Let $u(t)$ denote a control input trajectory over a horizon $[t_0, t_0 + T]$. The digital twin predicts a distribution over future pressures and gas distributions by propagating the posterior particles forward under $u(t)$. A risk-sensitive objective can be expressed as the expected penalty of violating pressure bounds and of excessive gas volume near the surface:

$$J(u) = \mathbb{E}\left[\int_{t_0}^{t_0+T} \Phi\big(p_{bh}(t), p_{shoe}(t), \alpha_{surf}(t)\big)\, dt\right] + \mathcal{R}(u), \tag{21}$$

where p_{bh} denotes bottomhole pressure, p_{shoe} a representative casing-shoe pressure, α_{surf} a surface-segment void fraction indicator, Φ is a smooth penalty encoding safety margins, and $\mathcal{R}(u)$ regularizes actuation magnitude and variability. Because regime affects friction and slip, and solubility affects free-gas fraction, the predicted distributions under $u(t)$ can differ materially from those produced by simpler models [53]. The control problem is therefore not merely about shifting mean pressures but about shaping uncertainty and avoiding trajectories that amplify regime-induced variability.

A practical implementation uses a receding-horizon strategy in which a finite set of candidate control trajectories is evaluated by forward propagation of particles. Since the reduced model is differentiable, gradient-based refinement of control trajectories is possible, but uncertainty and nonsmooth operational constraints often motivate sampling-based optimization. The regime-aware closures influence control evaluation through two primary mechanisms [54]. One mechanism is frictional sensitivity: intermittent regimes can produce higher pressure drops for the same flow, which may reduce the allowable pump rate margin. Another mechanism is slip sensitivity: regimes with higher drift velocity transport gas upward faster, altering when gas reaches the surface and when exsolution might accelerate void fraction growth in soluble-gas cases.

Solubility coupling introduces a delayed-response phenomenon in which actions taken early can influence later gas release. For example, maintaining higher pressure in an upper segment can keep dissolved gas in solution longer, reducing near-surface bubble formation in the short term but potentially storing gas that may later exsolve if pressure drops [55]. Conversely, reducing pressure may trigger exsolution and increase interfacial area, accelerating dissolution if pressure is later raised, depending on saturation history. These coupled effects make it insufficient to treat gas as a purely compressible free phase. The digital twin's dissolved-gas state provides a memory that allows the controller to anticipate delayed gas release and to avoid control actions that inadvertently cause rapid regime transitions near the surface.

Regime uncertainty alters control selection by changing the distribution of predicted pressure gradients and transport speeds [56]. If the vision module indicates high confidence in a dispersed bubbly regime, predicted friction and slip may be relatively stable, and more aggressive circulation may be feasible within safety margins. If uncertainty is high or churn-like intermittency is likely, the predicted pressure distribution widens, and a risk-sensitive controller would choose more conservative actuation to reduce the probability of constraint violation. This is a key advantage of treating regime probabilistically: the controller can explicitly account for ambiguity rather than acting on a potentially erroneous hard classification.

The same probabilistic machinery also supports diagnostic decisions about sensing [57]. If the controller's value function is sensitive to regime uncertainty at a particular axial region, then obtaining additional visual or other regime-informative measurements there has high expected value. Even in laboratory studies, this perspective guides camera placement and frame rate choices. In broader settings, it motivates adaptive sensing strategies that allocate bandwidth to locations where regime ambiguity most affects mitigation decisions. While such sensing policies are beyond the scope of the present implementation, the digital twin provides the quantitative foundation needed to compute such values of information [58].

It is important to emphasize that the control framing here is aimed at demonstrating the integration of prediction, uncertainty, and regime-aware closures. The paper does not attempt to encode field procedures or to provide operational instructions. Instead, it provides a modeling and inference layer that can be paired with existing safety protocols and decision frameworks, supplying better-calibrated forecasts of pressure and gas distribution under alternative actuation scenarios [59].

8. Discussion: Identifiability, Generalization, and Failure Modes

A regime-aware physics–vision digital twin introduces new capabilities but also new failure modes. Understanding identifiability is central. With pressure-only measurements, the inverse problem of recovering gas distribution and influx history is ill posed because multiple combinations of void fraction and friction can produce similar pressure gradients. Introducing regime as a latent variable increases flexibility, which can worsen identifiability unless constrained by priors or additional observations [60]. The latent-regime relaxation dynamics provides one such constraint, but it must be tuned to avoid over-regularization that prevents necessary regime changes. When vision observations are available, identifiability improves because regime is partially observed, reducing the degree to which the filter can trade off void fraction against friction. However, the improvement depends on calibration; an overconfident vision model can force incorrect regime inference and thereby bias the physical state estimates.

Generalization across gas types and fluids is another challenge [61]. The solubility model relies on an equilibrium function $c^*(p)$ and on effective mass-transfer coefficients. While the framework can represent differences through parameters, accurate prediction requires that parameter ranges be plausible. The paper addresses this by treating key solubility parameters as uncertain and inferrable when data provide evidence, rather than fixed constants. Nonetheless, certain combinations of limited sensors and strong

solubility effects can remain weakly identifiable [62]. In such cases, the digital twin is expected to report broader uncertainty, and control strategies should be risk-sensitive to that uncertainty.

The vision model faces domain shift when imaging conditions, fluids, or geometry differ from the training distribution. The inclusion of epistemic uncertainty is intended to detect such shifts, but uncertainty estimation is not perfect. A failure mode occurs when the model is confidently wrong due to spurious correlations in the training data [63]. The proposed ensemble-based uncertainty helps mitigate but does not eliminate this risk. The integration strategy therefore avoids hard coupling: vision outputs shape regime weights through a likelihood term whose strength is modulated by uncertainty, and the physics prior can resist implausible rapid regime changes. Additionally, the physical model provides cross-checks. If the vision module predicts a regime implying high slip and low friction, but pressure data indicate large gradients inconsistent with that, the filter can downweight the vision likelihood implicitly through residuals and can shift regime weights toward states consistent with both modalities [64].

Reduced-order physics introduces approximation error, especially for intermittent flows. The variance proxy σ_p^2 is a partial remedy, but it does not capture coherent oscillations that may matter over short timescales. In laboratory conditions with high-speed imaging and dense pressure sensors, such oscillations could be resolved and modeled explicitly, but in real-time inference with sparse sensors they are more appropriately treated statistically. The framework's probabilistic nature is a strength here, as it allows unresolved dynamics to be expressed as uncertainty rather than forcing a deterministic but misleading prediction [65].

Numerical stability and differentiability impose additional constraints. The use of smooth absolute values and convex blending improves stability but can slightly smear sharp transitions. This tradeoff is acceptable for inference and control, where robustness and calibration are often more valuable than reproducing every sharp feature. When sharper transitions are needed, the regime timescale τ_r can be reduced, and the softmax temperature can be adjusted to permit near-discrete regime weights while maintaining differentiability [66].

Finally, the framework's modularity is important. The reduced two-fluid core can be replaced by more detailed models when computation allows, and the vision module can be replaced by other regime-informative sensors when imaging is not available. The central idea remains: treat regime as a latent probabilistic variable that conditions closures and is inferred jointly with physical states, rather than as an external label imposed by a brittle map or as an ignored complexity absorbed into tuning constants.

9. Conclusion

This paper developed a regime-aware physics–vision digital twin for annular gas-kick migration that integrates reduced two-fluid dynamics, solubility-mediated mass transfer, differentiable closure blending, and probabilistic computer-vision regime inference [67]. The central modeling stance is to represent flow regime as a latent, uncertain field that is advected and relaxed under physical priors while being corrected by observational evidence. This representation enables smooth switching of slip, friction, and mass-transfer closures without discontinuities that would destabilize real-time inference. The inclusion of a dissolved-gas state provides a memory effect that captures dissolution at depth and exsolution near the surface, improving interpretability and forecasting in cases where solubility alters the apparent free-gas volume fraction.

A probabilistic vision observation model was framed as a likelihood over regime weights and auxiliary continuous proxies, with explicit uncertainty calibration to reduce the risk of overconfident misclassification driving erroneous closure selection [68]. The resulting sensor fusion problem was cast as constrained Bayesian filtering, supporting joint estimation of influx history, gas distribution, dissolved fraction, and regime field from pressure and visual data. The digital twin was then connected to mitigation-oriented prediction and control through posterior forward propagation and risk-sensitive evaluation of candidate actuation trajectories, emphasizing how regime uncertainty and solubility coupling can alter safety margins.

While reduced-order assumptions and domain shift remain practical concerns, the framework provides a coherent pathway to combine mechanistic constraints with learned perception, yielding predictions that are both physically grounded and informed by direct morphological evidence. The overall approach is intended to support robust monitoring and decision-making in transient annular two-phase events by improving closure adaptivity, uncertainty quantification, and the integration of heterogeneous sensing modalities [69].

References

[1] M. Stanislawek and J. R. Smith, "Analysis of alternative well-control methods for dual-density deepwater drilling," IADC/SPE Drilling Conference, 2 2006.

[2] A. Sherwood, "Explosive stimulation of a geothermal steam reservoir.," 1 1972.

[3] C. Hoyer, S. Fried, and D. Sask, "Test, treat, test system using a concentric coiled tubing/dst package," in Annual Technical Meeting, PETSOC, 6 1996.

[4] F. Verga and V. Rocca, "Green methodologies to test hydrocarbon reservoirs," American Journal of Environmental Sciences, vol. 6, pp. 1–10, 1 2010.

[5] T. R. Salakhov, V. Dubinsky, and V. U. Yamaliev, "A field-proven methodology for real-time drill bit condition assessment and drilling performance optimization," in SPE Russian Oil and Gas Technical Conference and Exhibition, SPE, 10 2008.

[6] C. E. Obi, A. R. Hasan, L. Abril, K. Manikonda, and A. Rahman, "Experimental investigation of gas kick behavior during shut-in condition," in ASTFE Digital Library, Begel House Inc., 2022.

[7] C. E. Obi, K. Manikonda, L. Abril, A. R. Hasan, and M. A. Rahman, "Dynamics of gas kick migration in the annulus while drilling/circulating," in International Conference on Offshore Mechanics and Arctic Engineering, vol. 85956, p. V010T11A089, American Society of Mechanical Engineers, 2022.

[8] T. Fang, F. Ren, H. Liu, Y. Zhang, and J. Cheng, "Progress and development of particle jet drilling speed-increasing technology and rock-breaking mechanism for deep well," Journal of Petroleum Exploration and Production Technology, vol. 12, pp. 1697–1708, 12 2021.

[9] "Department of petroleum engineering and center for petroleum and geosystems engineering annual report, 1990–1991 academic year," 12 1991.

[10] A. Mahmood, L. Ring, A. Alajbegovic, and S. Nienhuis, "Enabling new techniques: Nitrogen gas qualification and testing of a rotating control device," in IADC/SPE Managed Pressure Drilling & Underbalanced Operations Conference & Exhibition, SPE, 3 2017.

[11] J. J. Lewis, "New uses of existing technology for controlling blowouts: Chronology of a blowout offshore louisiana," Journal of Petroleum Technology, vol. 30, pp. 1473–1480, 10 1978.

[12] "Project rio blanco: detonation related activities. final report," 6 1975.

[13] C. Wei, Y. Chen, O. Santos, M. Kunju, S. Mahmud, M. Almeida, and P. Sonnemann, "An evaluation of pressure control methods during riser gas handling with mpd equipment based on transient multiphase flow modeling and distributed fiber optic sensing," in SPE Annual Technical Conference and Exhibition, SPE, 9 2022.

[14] R. Qin, B. Xu, H. Chen, Q. Lu, C. Li, J. Wang, Q. Feng, X. Liu, and L. Wang, "Qualitative and quantitative analysis of the stability of conductors in riserless mud recovery system," Energies, vol. 15, pp. 7657–7657, 10 2022.

[15] "Prairie canal well no. 1, calcasieu parish, louisiana. volume 1. completion and testing. final report," 1 1981.

[16] F. Rigby and P. Reardon, "Benefit/cost analysis for research in geothermal log interpretation. final report," 7 1979.

[17] M. de Wit, "Ultra-deep drilling through 3.5-billion-year-old crust in south africa," Scientific Drilling, vol. 11, pp. 66–73, 3 2011.

[18] "Preliminary performance assessment for the waste isolation pilot plant, december 1992. volume 2, technical basis," 12 1992.

[19] M. E. Loginova and F. A. Agzamov, "Viscoelastic systems for well construction," Kazakhstan journal for oil & gas industry, vol. 4, pp. 58–68, 5 2022.

[20] M. Naeem and J. Chinn, "Advancement in laser drilling for aerospace gas turbines," in PICALO 2008: 3rd Pacific International Conference on Laser Materials Processing, Micro, Nano and Ultrafast Fabrication, vol. 2008, pp. 197–202, Laser Institute of AmericaLIA, 4 2008.

[21] C. R. Neal, M. F. Coffin, N. T. Arndt, R. A. Duncan, O. Eldholm, E. Erba, C. Farnetani, J. F. Fitton, S. P. Ingle, N. Ohkouchi, M. R. Rampino, M. K. Reichow, S. Self, and Y. Tatsumi, "Investigating large igneous province formation and associated paleoenvironmental events: A white paper for scientific drilling," Scientific Drilling, vol. 6, pp. 4–18, 7 2008.

[22] C. Helmer, A. Churcher, G. Mclvor, and R. Shields, "Arctic offshore development: Managing the risk," in Offshore Technology Conference, OTC, 5 1994.

[23] Y. Guimin, J. Hao, and K. Qingwen, "Study on hydrate risk in the water drainage pipeline for offshore natural gas hydrate pilot production," Frontiers in Earth Science, vol. 9, 2 2022.

[24] J. L. Smalley, "A safety equipment list for rotary mode core sampling systems operation in single shell flammable gas tanks," 5 1999.

[25] J. Sullivan, C. Clark, L. Yuan, J. Han, and M. Wang, "Life-cycle analysis results for geothermal systems in comparison to other power systems: Part ii.," 11 2011.

[26] W. C. Maurer, C. G. Ruan, and G. Deskins, "Joint-industry partnership to develop a hollow sphere dual-gradient drilling system," 5 2003.

[27] P. Dobrokhleb, V. Kretsul, S. Dymov, M. Razumniy, A. Ablaev, A. Milenkiy, and O. Tarasov, "Engineered drilling system approach makes the impossible possible: A case study of horizontal well drilling in achimov formations of urengoyskoe field," in SPE Russian Petroleum Technology Conference, SPE, 10 2015.

[28] P. O'bryan, "Well control problems associated with gas solubility in oil-based drilling fluids.," 1 1988.

[29] X. Kong, Y. Lin, Y. Qiu, H. Zhu, L. Dong, and Y. Chen, "A new model for predicting dynamic surge pressure in gas and drilling mud two-phase flow during tripping operations," Mathematical Problems in Engineering, vol. 2014, pp. 1–16, 1 2014.

[30] A. Mohamad, N. Yusoff, S. Aris, D. Bismo, and M. Regan, "Dare to change: An approach to implement enterprise level of real time well solution for collaborative working environment," in IADC/SPE Asia Pacific Drilling Technology Conference, SPE, 8 2016.

[31] C. Goranson, "Applicability of petroleum horizontal drilling technology to hazardous waste site characterization and remediation," 9 1992.

[32] C. Carpenter, "Matrix injectivity achieved in deepwater gas-injector wells," Journal of Petroleum Technology, vol. 74, pp. 62–64, 5 2022.

[33] L. Brown and A. Vadie, "The utilization of the microflora indignous to and present in oil-bearing formations to selectively plug the more porous zones thereby increasing oil recovery during waterflooding," 4 1997.

[34] K. Manikonda, C. Obi, A. A. Brahmane, M. A. Rahman, and A. R. Hasan, "Vertical two-phase flow regimes in an annulus image dataset-texas a&m university," Data in Brief, vol. 58, p. 111245, 2025.

[35] T. I. Gataullin, P. I. Eliseev, F. S. Zavalin, and A. A. Lutfullin, "Selection of the optimal type of fractured well completion based on simulation of highly heterogeneous reservoir (russian)," in SPE Russian Oil and Gas Exploration and Production Technical Conference and Exhibition, SPE, 10 2012.

[36] M. Luo, L. Yang, H. Wen, D. Zhao, and K. Wang, "Numerical optimization of drilling parameters for gas predrainage and excavating-drainage collaboration on roadway head," Geofluids, vol. 2022, pp. 1–10, 5 2022.

[37] T. L. McLing, M. Carpenter, W. Brandon, and B. Zavala, "Testing novel cr-39 detector deployment system for identification of subsurface fractures, soda springs, id," 6 2015.

[38] R. Mann, "Slant hole completion test. final report," 7 1993.

[39] Y. Zhang, W. Wang, P. Zhang, G. Li, S. Tian, J. Lu, and B. Zhang, "A solution to sand production from natural gas hydrate deposits with radial wells: Combined gravel packing and sand screen," Journal of Marine Science and Engineering, vol. 10, pp. 71–71, 1 2022.

[40] F. Huszarik, J. Reichman, and C. Jb, "Use of high-pressure waterjets in utility industry applications," Erosion: Prevention and Useful Applications, pp. 597–615, 1 1979.

[41] J. L. Gillette and R. L. Kolpa, "Overview of interstate hydrogen pipeline systems.," 2 2008.

[42] D. Marum, A. Cartellieri, E. Shahini, and D. Scanavino, "A novel and sustainable generation of advanced mud gas logging system for managed pressure drilling applications: An explorative well deployment from north germany," in SPE Middle East Oil & Gas Show and Conference, SPE, 12 2021.

[43] "Resource engineering and economic studies for direct application of geothermal energy. draft final report," 12 1981.

[44] K. C. Manger, "Assessing geothermal energy potential in upstate new york. final report, tasks 1, 3, and 4," 7 1996.

[45] B. Patel, T. D. Cooper, and W. Billings, "The application of advanced gas extraction and analysis system complements early kick detection & control capabilities of managed pressure drilling system with added hse value," SPE/IADC Drilling Conference, 3 2013.

[46] D. Wu, J. Gao, and K. Lu, "Dust control technology in dry directional drilling in soft and broken coal seams," Energies, vol. 15, pp. 3804–3804, 5 2022.

[47] M. Kang, S. Christian, M. A. Celia, D. L. Mauzerall, M. Bill, A. R. Miller, Y. Chen, M. E. Conrad, T. H. Darrah, and R. B. Jackson, "Identification and characterization of high methane-emitting abandoned oil and gas wells," Proceedings of the National Academy of Sciences of the United States of America, vol. 113, pp. 13636–13641, 11 2016.

[48] "Geothermal energy program overview: Fiscal year 1991," 12 1991.

[49] L. E. Capuano, M. Huh, R. J. Swanson, D. W. Raymond, J. T. Finger, A. J. Mansure, Y. Polsky, and S. D. Knudsen, "Enhanced geothermal systems (egs) well construction technology evaluation report.," 12 2008.

[50] J. Zeng, G. Chen, K. Zhu, J. Mo, and C. Li, "The research on bulk system transfer ability of cpoe-16 jack-up," in Volume 4A: Pipeline and Riser Technology, American Society of Mechanical Engineers, 6 2013.

[51] M. M. Rajabi, B. Rohde, N. Maguire, R. S. Stave, and R. Tapper, "Successful implementations of tophole managed pressure cementing and managed pressure drilling in the caspian sea," in SPE/IADC Managed Pressure Drilling and Underbalanced Operations Conference and Exhibition, SPE, 3 2012.

[52] Z. He, L. Juncheng, Z. Zhijun, and L. Wei, "Research on safety monitoring system of bottom hole pressure in coalbed methane underbalanced drilling process," The Open Fuels & Energy Science Journal, vol. 8, pp. 197–201, 9 2015.

[53] B. W. Atchison, "Automated well control: From automated detection to automated shut-in," in SPE/IADC Middle East Drilling Technology Conference and Exhibition, SPE, 5 2021.

[54] A. K. Raptanov, V. V. Ruzhenskyi, B. I. Kostiv, M. A. Myslyuk, and V. M. Charkovskyy, "Analysis of the deep drilling technology in unstable formations at the semyrenky gas condensate field," SOCAR Proceedings, pp. 52–64, 12 2021.

[55] M. Zulqarnain and M. Tyagi, "Quantitative risk assessment (qra) of an exploratory drilling oil spill in deepwater gulf of mexico," in Volume 5: Materials Technology; Petroleum Technology, American Society of Mechanical Engineers, 6 2014.

[56] M. Stanislawek, "Analysis of alternative well control methods for dual density deepwater drilling," 11 2004.

[57] R. Rickman, D. B. Allison, M. A. Mccabe, and J. Jansen, "Development of a formation compatible fluid system for creating fracture isolation points," in SPE Eastern Regional Meeting, SPE, 9 2009.

[58] Z. Shi, D. Ye, J. Hao, B. Qin, and G. Li, "Research on gas extraction and cut flow technology for lower slice pressure relief gas under slice mining of extra-thick coal seam.," ACS omega, vol. 7, pp. 24531–24550, 7 2022.

[59] S. Neacşu and R. Rădulescu, "Increasing calculation accuracy in the design stage of a gas transportation system," Analele Universitatii "Ovidius" Constanta - Seria Chimie, vol. 24, pp. 61–66, 12 2013.

[60] M. Yeo, A. J. Macgregor, H. Pinkstone, and B. Piccolo, "Offshore deepwater managed pressure drilling and riser gas handling equipment design," in SPE/IADC Managed Pressure Drilling and Underbalanced Operations Conference & Exhibition, SPE, 4 2015.

[61] A. Beswick, J. Scarrow, and W. Muller-Ruhe, "The integration of oilfield, mining and geotechnical exploration technologies for a deep scientific investigation to depths up to 2000 m," IADC/SPE Drilling Conference, 2 1992.

[62] "Eia model documentation: Documentation of the oil and gas supply module (ogsm)," 1 1997.

[63] Z. Shang, Z. Wang, Z. Cheng, H. Wang, L. Chen, L. Li, J. Fu, and H. Liu, "Permeability enhancement technology for soft and low-permeability coal seams combined with hydraulic perforation and hydraulic fracturing," Geofluids, vol. 2022, pp. 1–13, 7 2022.

[64] D. S. Pixton, R. A. Shishavan, H. D. Perez, J. D. Hedengren, and A. D. Craig, "Addressing ubo and mpd challenges with wired drill pipe telemetry," in SPE/IADC Managed Pressure Drilling & Underbalanced Operations Conference & Exhibition, SPE, 4 2014.

[65] J. E. Vasquez, "A novel temperature-activated, rigid-setting material: Case histories for drilling and conformance offshore applications," in OTC Brasil, OTC, 10 2013.

[66] D. V. Eliseev, M. Y. Golenkin, A. Senkov, A. Latypov, I. Bulygin, A. Ruzhnikov, M. Buyanov, and A. Kashlev, "New vision: Ic taml5 wells on caspian offshore. reasons, implementation and results," in SPE Russian Petroleum Technology Conference and Exhibition, SPE, 10 2016.

[67] A. J. Hinton, T. Nolan, V. Tilley, and B. Eikemo, "Taming the grebe sand—tophole drilling success in the ichthys field," in Asia Pacific Oil and Gas Conference & Exhibition, SPE, 8 2009.

[68] P. L. Younger, "Geothermal energy: delivering on the global potential," Energies, vol. 8, pp. 11737–11754, 10 2015.

[69] C. R. Johnson, S. Sari, A. Ahrenst, and I. Gozubuyuk, "Energy transition by employing a self-healing, reduced carbon dioxide footprint sealant in a strategic underground gas storage project," in SPE EuropEC - Europe Energy Conference featured at the 83rd EAGE Annual Conference & Exhibition, SPE, 6 2022.